Supporting Information

For

Enhanced electrochemical supercapacitors from the metal silicates (Zn, Mn, Ni and Co) by multi-step treatment of natural green algaes

Shaoqing Zhang [a,b] *, Aixue Wang [a], Guozhong Zhang [a], Aoqi Mei [a], Tianming Lv [c], Xuchun Wang [a,b], Hanmei Jiang [d] *

[a] College of chemistry and materials engineering, Anhui Science and Technology University, Bengbu 239000, China

[b] Anhui Province Quartz Sand Purification and Photovoltaic Glass Engineering Research Center, Anhui Science and Technology University, Bengbu 239000, China

[c] Instrumental Analysis Center, Dalian University of Technology, Dalian 116024, China

[d] Hubei Key Laboratory of Pollutant Analysis &Reuse Technology, College of Chemistry and Chemical Engineering, Hubei Normal University, Huangshi 435002, China

* Corresponding author. E-mail address: zhangsq@ahstu.edu.cn (S. Zhang); 20230125@hbnu.edu.cn (H. Jiang)

Reagents and starting materials

Zinc (II) acetate dihydrate ($Zn(OAc)_2 \cdot 2H_2O$), manganese (II) acetate tetrahydrate ($Mn(OAc)_2 \cdot 4H_2O$), nickel (II) acetate tetrahydrate ($Ni(OAc)_2 \cdot 4H_2O$), cobalt (II) acetate tetrahydrate ($Co(OAc)_2 \cdot 4H_2O$), hydrochloric acid aqueous solution (HCl, 36.5 wt%), sodium chloride (NaCl), sodium hydroxide (NaOH) and ethanol were purchased from Aladin Chemical Reagent Co., Ltd. and used without any further purification. Fresh green algaes (GAs) were picked from a campus pond in Bengbu City, China. During this experiment, the green algaes were washed with deionized (DI) water and cut into pieces, and then dried at 60 °C for 12 h.

Material characterizations

X-ray diffraction (XRD) was used to identify the compositions and structures of the products using Bruker D8 Discover X-ray diffractometer with Cu Kα radiation (50 kV, 1000 mA). Raman spectra were recorded on a Renishaw InVia Raman microscope with a laser excitation sources of 532 nm. Fourier transform infrared spectroscopy (FTIR) spectra were collected on a Nicolet 6700 spectrometer from 4000 to 400 cm^{-1} using the KBr pellet technique. X-ray photoelectron spectrum (XPS) was taken on a Thermo ESCALAB 250XiX spectrometer with monochromatized Al Kα X-ray (hν = 1486.6 eV). Inductively Coupled Plasma (ICP, PerkinElmer, Optima 2000DV) was adopted to analyze the content of metal elements. A linear relationship was assumed between the edge position and oxidation state. The microstructures and chemical compositions of the products were characterized by a field-emission scanning electron microscope (FE-SEM, FEI Sirion) with an Energy-dispersive X-ray spectrometer (EDS) and transmission electron microscopy (TEM, JEOL-JEM2100F). The Brunauer-Emmet-Teller (BET) surface areas of the samples were determined by a Micromeritics ASAP-2020 porosity analyzer after being degassed at 150 ℃ for 10 h.

Electrochemical characterizations

The working electrodes were prepared by mixing active materials, carbon black and polyvinylidenedifluoride (PVDF) together in a weight of 8:1:1. Then a small quantity of N-methyl-2-pyrrolidone (NMP) was dropwise added into the mixture to dissolve it homogeneously. The

mixed slurry was then coated onto a nickel foam with an area of 1×1 cm^2 and dried at 100 °C for 24 h to remove organic solvent, then pressed under a pressure of 10 MPa for 10 min to obtain the working electrode. The mass loading of active materials on the nickel foam was typically 3-4 mg cm^{-2}. Electrochemical characterization was carried out in a three-electrode system in 3 M KOH aqueous solution, where Hg/HgO and carbon rod were regarded as the reference electrode and the counter electrode, respectively. The flexible solid-state asymmetric supercapacitors (HSCs) were constructed from working electrode and activated carbon (AC) electrode using a membrane filter (NKK-PF30AC) as a separator. Both of the electrodes were prepared in the same way as that used for the preparation of the working electrode in the three-electrode system. For the purpose of getting a better performance of the device, the mass ratio of the positive to negative electrode is balanced on the basis of the equal charge between cathode and anode. The electrolyte was used 3 $mol \cdot L^{-1}$ polyvinyl alcohol/KOH (PVA/KOH) gel electrolyte. After dipping in the electrolyte, the entire device was sealed in plastic sheet to avoid the evaporation of electrolyte. The electrochemical characteristics of the ASCs devices were evaluated by galvanostatic charge-discharge (GCD), cyclic voltammetry (CV) and electrochemical impedance spectroscopy (EIS) measurements. The contribution of the nickel foam to the capacitance can be negligible [1]. The specific capacitance (C) of a single electrode was calculated on the basis of GCD according to the equation (1-2):

$$Cs = \frac{I \cdot \Delta t}{s \cdot \Delta V} \quad (1)$$

$$C = \frac{I \cdot \Delta t}{m \cdot \Delta V} \quad (2)$$

Where Cs (mF cm^{-2}) and C (F g^{-1}) represent areal and specific capacitance, respectively; I (A) denotes discharge current; Δt (s) signifies discharge time; s (cm^{-2}) corresponds to the area of working electrode; m (g) corresponds to the mass of the active material in the working electrode, and ΔV (V) refers to the potential window. The areal capacitance, areal capacity, energy density and power density of the ASC device were calculated on the basis of the equations (3-4):

$$E = \frac{1}{2} Cs \cdot (\Delta V)^2 \quad (3)$$

$$P = \frac{E}{\Delta t} \quad (4)$$

Where E ($Wh \cdot m^{-2}$) is the energy density and P ($W \cdot m^{-2}$) is the power density, respectively.

Figure S1

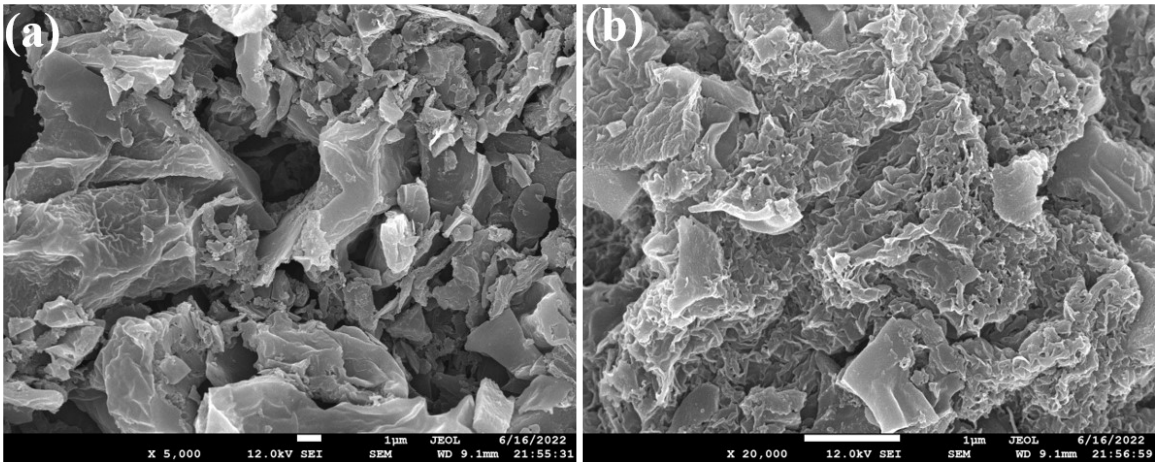

Fig. S1. FE-SEM images of C-SiO_2 from green algaes.

Figure S2

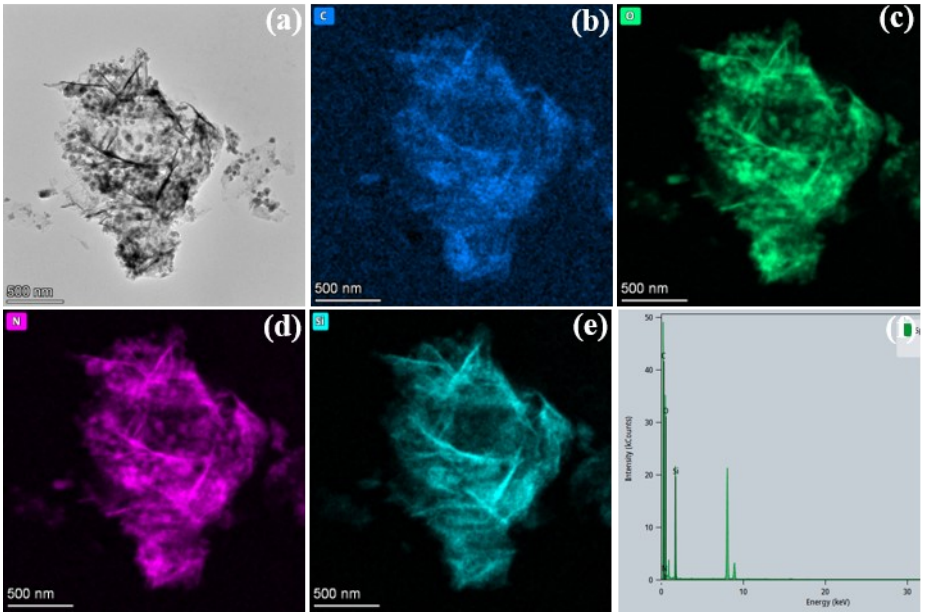

Fig. S2. TEM and Elemental mapping images of C-SiO_2 (a-e) and EDS layered image (f).

Figure S3

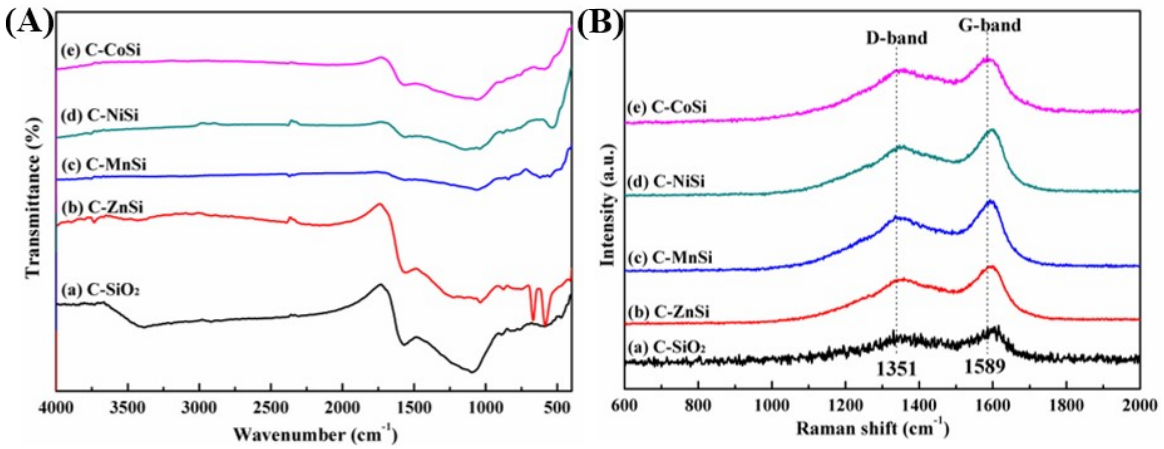

Fig. S3. (A) FT-IR spectra and (B) Raman spectra of the materials.

Figure S4

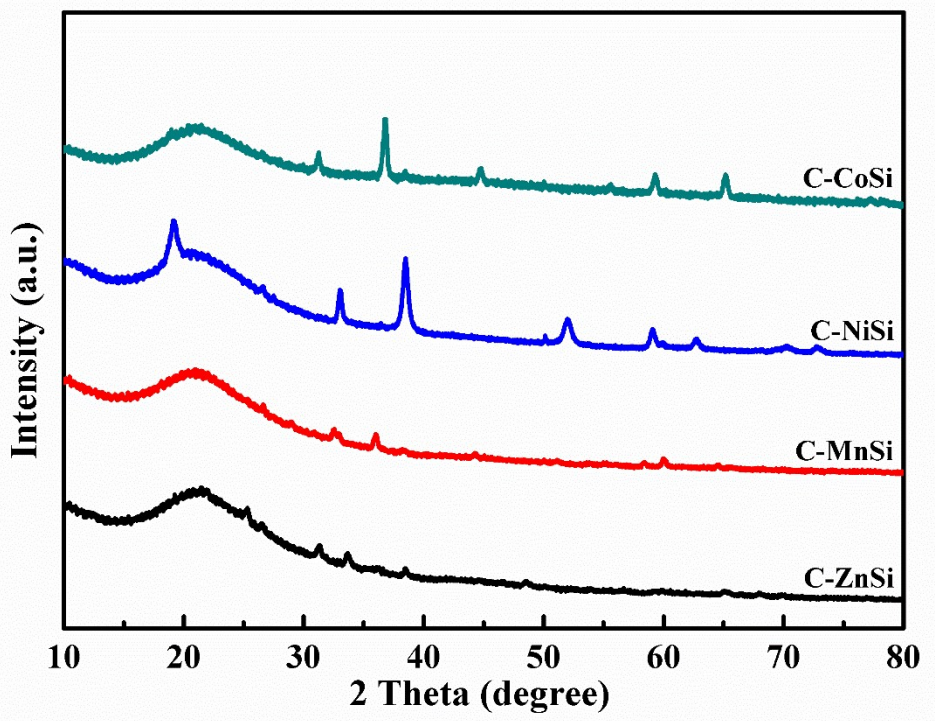

Fig. S4. XRD patterns of the synthesized C-ZnSi, C-MnSi, C-NiSi and C-CoSi.

Figure S5

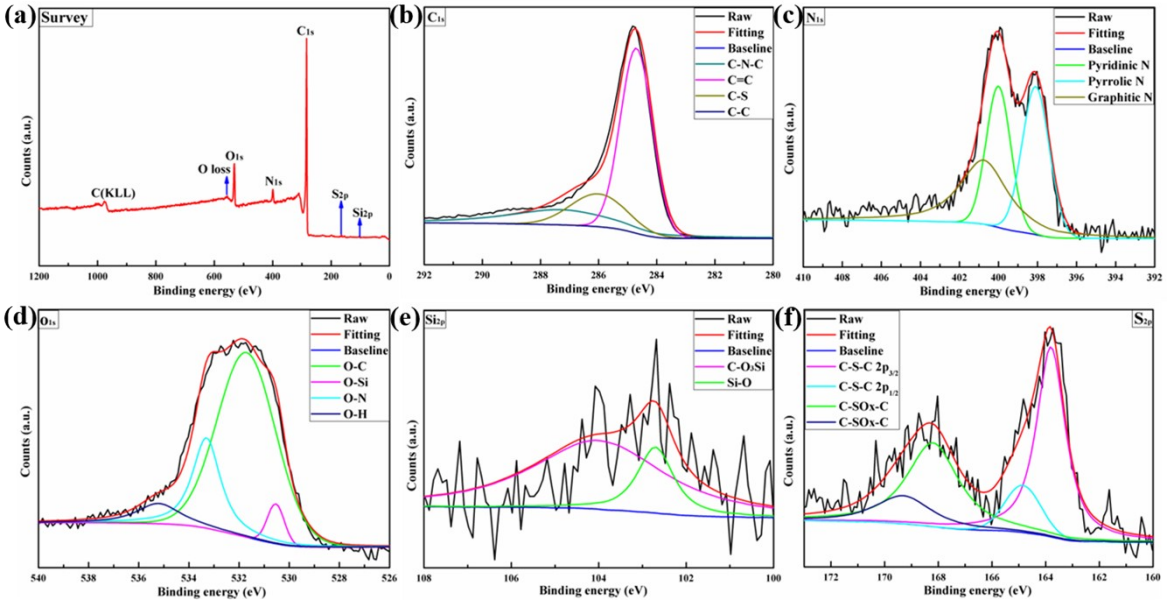

Fig. S5. XPS spectra of C-SiO_2: (a) full spectrum, (b) C_{1s}, (c) N_{1s}, (d) O_{2p}, (e) Si_{2p} and (f) S_{2p}.

Figure S6

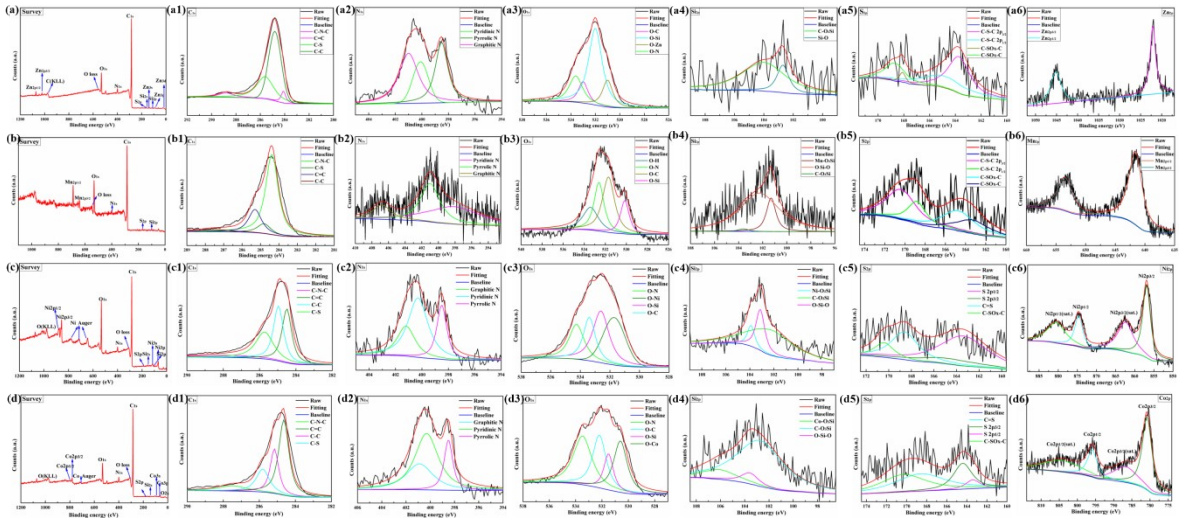

Fig. S6. XPS spectra of C-MSi: (a-d) full spectrum, (a1-d1) C_{1s}, (a2-d2) N_{1s}, (a3-d3) O_{2p}, (a4-d4) Si_{2p}, (a5-d5) S_{2p} and (a6-d6) M_{2p} (M = Zn, Mn, Ni and Co).

Figure S7

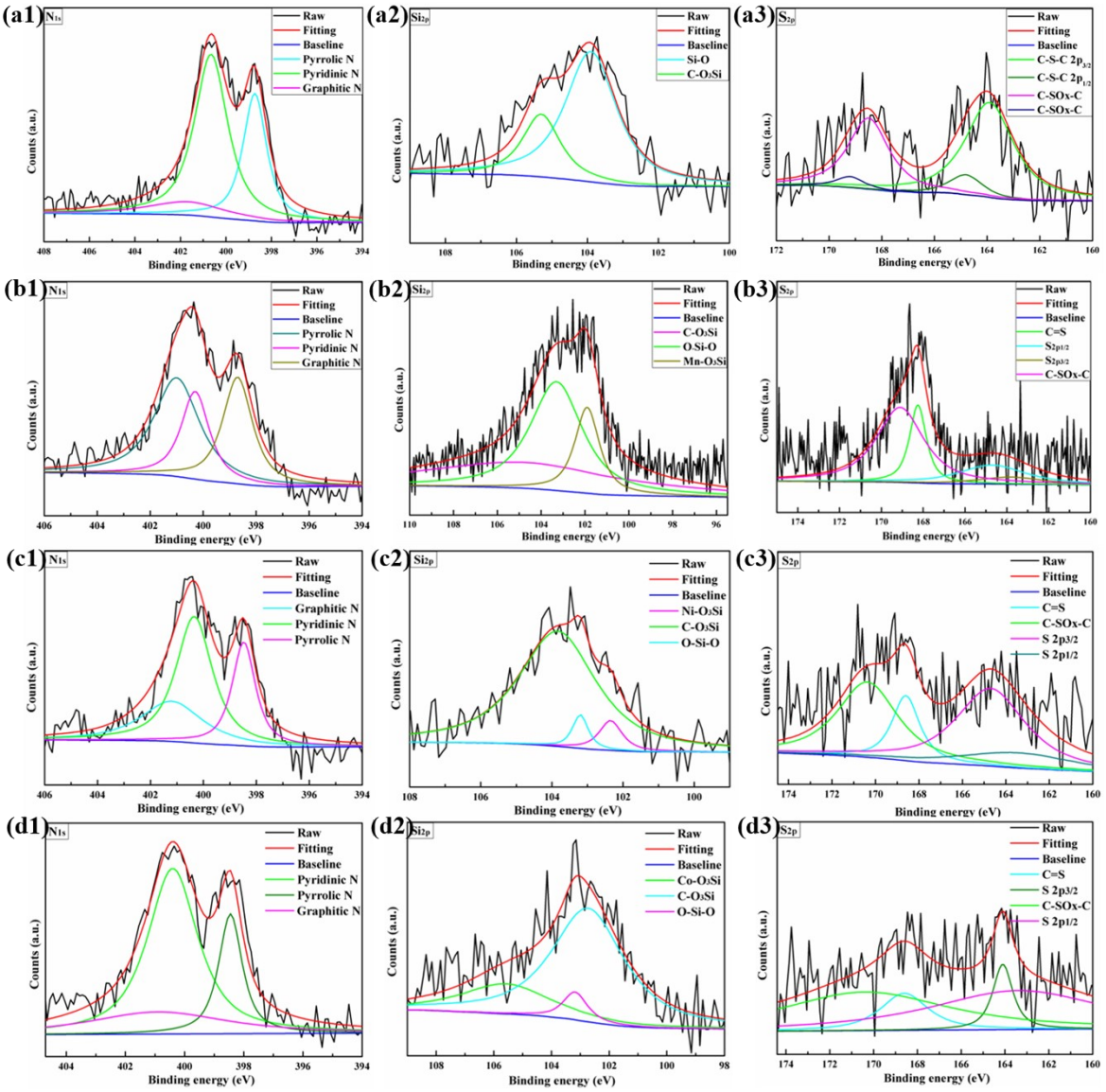

Fig. S7. XPS spectra of m-C-MSi: (a1-d1) N_{1s}, (a2-d2) Si_{2p} and (a3-d3) S_{2p} (M = Zn, Mn, Ni and Co).

Figure S8

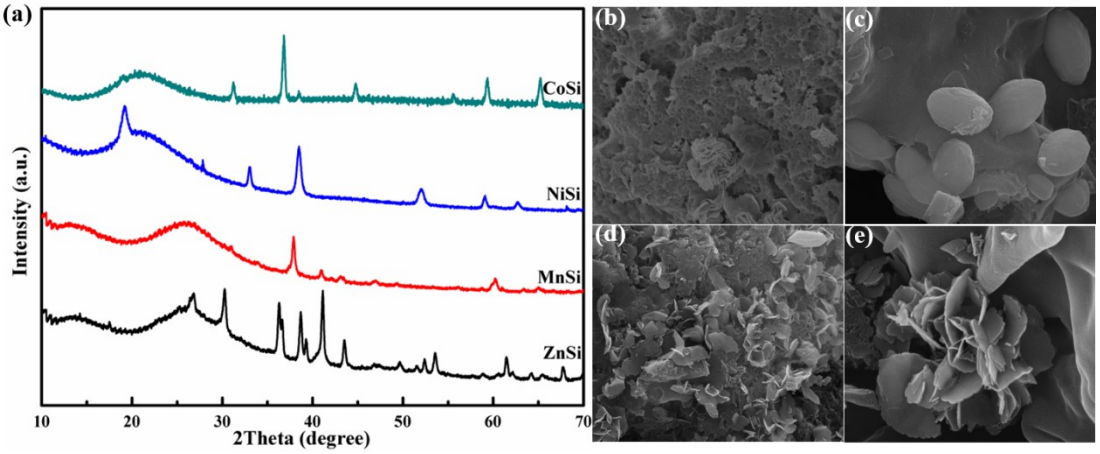

Fig. S8. (a) XRD patterns of the synthesized ZnSi, MnSi, NiSi and CoSi; FE-SEM images of ZnSi (b), MnSi (c), NiSi (d) and CoSi (e).

SiO_2 was used as the silicon source to synthesize the metal silicates and named as ZnSi, MnSi, NiSi and CoSi, respectively. The XRD patterns and FE-SEM images are shown in Fig. S8. Compared to the m-C-MSi materials, the crystallinity of these materials has been enhanced, and there is no significant change in morphology.

Figure S9

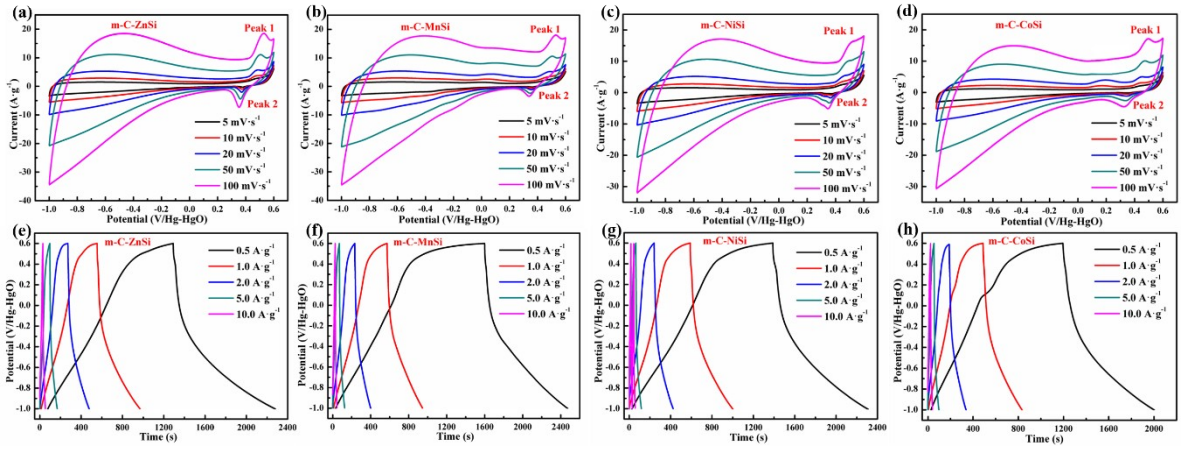

Fig. S9. (a-d) CV curves of m-C-MSi at different scan rates from 5 mV s^{-1} to 100 mV s^{-1}; (e-h) GCD curves of C-MSi at different current densities from 0.5 A g^{-1} to 10.0 A g^{-1} (M = Zn, Mn, Ni, Co).

Figure S10

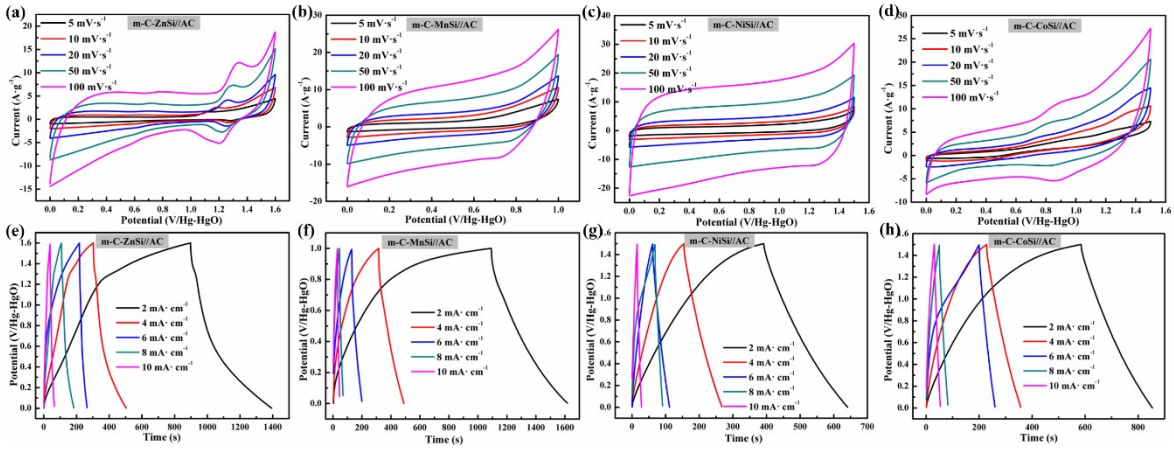

Fig. S10. (a-d) CV curves of m-C-MSi//AC at different scan rates from 5 mV s^{-1} to 100 mV s^{-1}; (e-h) GCD curves of m-C-MSi-3//AC at different current densities 2 mA cm^{-2} to 10.0 mA cm^{-2} (M = Zn, Mn, Ni, Co).

Figure S11

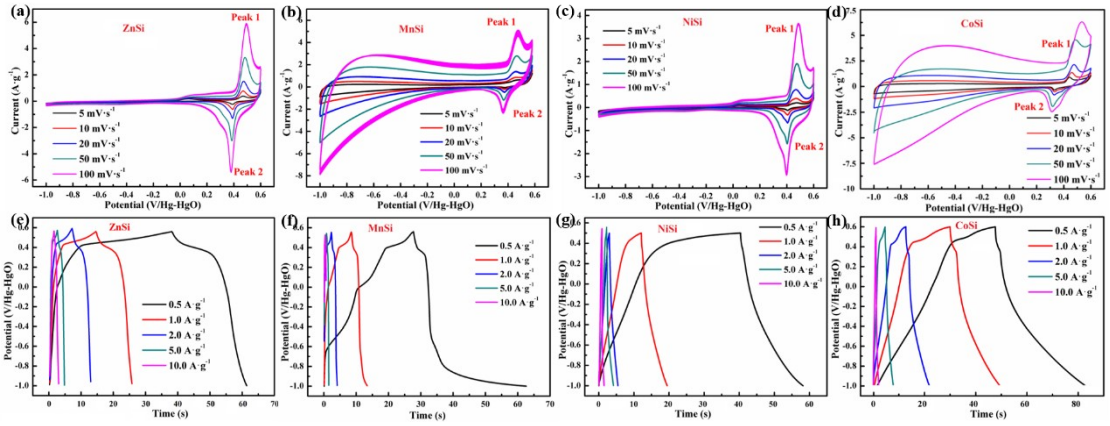

Fig. S11. (a-d) CV curves of MSi at different scan rates from 5 mV s^{-1} to 100 mV s^{-1}; (e-h) GCD curves of MSi at different current densities from 0.5 A g^{-1} to 10.0 A g^{-1} (M = Zn, Mn, Ni, Co).

For comparison, the CV curves and GCD curves tests of MSi (M = Zn, Mn, Ni and Co) shown in Fig. S11 present similar potential range and shape with very lower electrochemical performance.

Table S1

Table S1. Pore Parameters of m-C-MSi (M = Zn, Mn, Ni and Co).

sample	BET surface area (m^2 g^{-1})	total pore vol (cm^3 g^{-1})	Average pore diameter (nm)
m-C-ZnSi	604	0.596	4.09
m-C-MnSi	617	0.588	5.67
m-C-NiSi	599	0.581	4.03
m-C-CoSi	581	0.562	3.91

Table S2

Table S2. Comparison of the electrochemical performance of m-C-ZnSi, m-C-MnSi, m-C-NiSi and m-C-CoSi with the reported silicate-based materials.

Si- or Zn-based materials	Electrolyte [a]	Potential/V	Capacitance/mF cm^{-2}	Cycling capability	Reference
$Ni_3Si_2O_5(OH)_4$/RGO	2 M KOH	0.2 ~ 0.6	178.9 F g^{-1}, 1 A g^{-1}	97.6 % after 5000	[2]
$MnSiO_3$	6 M KOH	0.2 ~ 0.6	251 F·g^{-1}, 0.6 A·g^{-1}	—	[3]
Manganese silicate drapes	1 M KOH	-0.5 ~ 0.4	283 F g^{-1}, 0.5 A g^{-1}	74.7 % after 1000	[4]
$(Ni, Co)_3Si_2O_5(OH)_4$	1 M KOH	0 ~ 0.5	144 F g^{-1}, 1 A g^{-1}	99.3 % after 10000	[5]
Mesoporous-Li_2MnSiO_4	2 M KOH	0 ~ 0.55	120 F g^{-1}, 20 mV·s^{-1}	85.7 % after 500	[6]
$Ni_3Si_2O_5(OH)_4$	3 M KOH	0 ~ 0.5	132.4 F g^{-1}, 0.5 A g^{-1}	100 % after 10000	[7]
$Co_3(Si_2O_5)_2(OH)_2$	6 M KOH	0.1 ~ 0.55	237 F g^{-1}, 5.7 mA cm^{-2}	95 % after 150	[8]
$Co_3Si_2O_5(OH)_4$	6 M KOH	0 ~ 0.5	570 F g^{-1}, 0.7 A g^{-1}	—	[9]
$MnSiO_3$/GO	1 M Na_2SO_4	-0.2 ~ 1	262.5 F g^{-1}, 0.5 A g^{-1}	53 % after 5000	[10]
$Co_xNi_{3-x}Si_2O_5(OH)_4$	3 M KOH	-0.80 ~ 0.6	226 F g^{-1}, 0.5 A g^{-1}	99 % after 10000	[11]
MnO_2/carbon cloth	0.1 M Na_2SO_4	0 ~ 0.8	230 mF cm^{-2}, 10 mV s^{-1}	98.5 % after 3000	[12]
CoSi hollow sphere	3 M KOH	0 ~ 0.5	452.8 F g^{-1}, 0.5 A g^{-1}	89 % after 10000	[13]
SWCNT/cellulose/PANI	1 M H_2SO_4	-0.2 ~ 0.6	330 mF cm^{-2}, 0.2 mA cm^{-2}	79% after 1000	[14]
$Zn_4Si_2O_7(OH)_2·H_2O$	3 M KOH	-1.0 ~ 0.6	341 mF cm^{-2}, 5 mV·s^{-1}	99 % after 10000	[15]
$Co_2Si_2O_4$	6 M KOH	0 ~ 0.5	267 mF cm^{-2}, 5 mV·s^{-1}	90 % after 10000	[16]
e-NiSi-3	6 M KOH	0 ~ 0.5	272 F·g^{-1} ,1 A·g^{-1}	96% after 10000	[17]
e-MnSi-3	6 M KOH	0 ~ 0.5	439 F·g^{-1} ,1 A·g^{-1}	80% after 10000	[17]
C-ZnSi-4	3 M KOH	-1.0 ~ 0.6	479 F g^{-1}, 0.5 A g^{-1}	84 % after 10000	[18]
C-MnSi-4	3 M KOH	-1.0 ~ 0.6	529 F g^{-1}, 0.5 A g^{-1}	86 % after 10000	[18]
e-C-ZnSi-4	3 M KOH	-1.0 ~ 0.6	527 F g^{-1}, 0.5 A g^{-1}	99 % after 10000	[18]
e-C-MnSi-4	3 M KOH	-1.0 ~ 0.6	571 F g^{-1}, 0.5 A g^{-1}	98 % after 10000	[18]
C-NiSi-3	3 M KOH	-1.0 ~ 0.6	401 F g^{-1}, 0.5 A g^{-1}	87 % after 10000	[19]
C-CoSi-3	3 M KOH	-1.0 ~ 0.6	373 F g^{-1}, 0.5 A g^{-1}	84 % after 10000	[19]
e-C-NiSi-3	3 M KOH	-1.0 ~ 0.6	439 F g^{-1}, 0.5 A g^{-1}	94 % after 10000	[19]
e-C-CoSi-3	3 M KOH	-1.0 ~ 0.6	402 F g^{-1}, 0.5 A g^{-1}	90 % after 10000	[19]
m-C-ZnSi	**3 M KOH**	**-1.0 ~ 0.6**	**548** F g^{-1}, 0.5 A g^{-1}	**99.4 % after 10000**	**This work**
m-C-MnSi	**3 M KOH**	**-1.0 ~ 0.6**	**590** F g^{-1}, 0.5 A g^{-1}	**99.1 % after 10000**	**This work**
m-C-NiSi	**3 M KOH**	**-1.0 ~ 0.6**	**487** F g^{-1}, 0.5 A g^{-1}	**99.6 % after 10000**	**This work**
m-C-CoSi	**3 M KOH**	**-1.0 ~ 0.6**	**453** F g^{-1}, 0.5 A g^{-1}	**99.3 % after 10000**	**This work**

a M = mol L^{-1}

Table S3

Table S3. Comparison of the electrochemical performance of the devices based on silicate-based materials.

Various devices	Electrolyte	Potential	Capacitance	Cycling capability	Energy density	Reference
C-ZnSi//AC ASC	PVA/KOH	2 V	194 mF cm^{-2}, 2 mA cm^{-2}	80% after 6900	0.690 Wh m^{-2}	[14]
CoNiSi/C//$Ni(OH)_2$ ASC	PVA/KOH	1.6 V	254 mF cm^{-2}, 2 mA cm^{-2}	82% after 10000	0.793 Wh m^{-2}	[4]
MnSi-C//$Ni(OH)_2$ ASC	PVA/KOH	2 V	439 mF cm^{-2}, 4 mA cm^{-2}	34% after 1000	5.3 mWh cm^{-3}	[2]
C-NiSi//$Ni(OH)_2$ ASC	PVA/KOH	1.8 V	694 mF cm^{-2}, 4 mA cm^{-2}	56% after 3000	6.78 mWh cm^{-3}	[6]
C/$Co_3Si_2O_5(OH)_4$//AC ASC	PVA/KOH	1.5 V	352 mF cm^{-2}, 1 mA cm^{-2}	97.2% after 6000	8.5 mWh cm^{-3}	[8]
NiSi//AC HSC	PVA/KOH	1.5 V	207 mF cm^{-2}, 4 mA cm^{-2}	79% after 5000	1.62 Wh m^{-2}	[16]
CoSi//AC HSC	PVA/KOH	1.5 V	135 mF cm^{-2}, 4 mA cm^{-2}	76% after 5000	1.05 Wh m^{-2}	[16]
MnSi//AC HSC	PVA/KOH	1.5 V	226 mF cm^{-2}, 4 mA cm^{-2}	58 % after 5000	1.77 Wh m^{-2}	[16]
C-ZnSi-4//AC HSC	PVA/KOH	1.6 V	576 mF cm^{-2}, 2 mA cm^{-2}	69.0 % after 5000	3.74 Wh m^{-2}	[18]
C-MnSi-4//AC HSC	PVA/KOH	1.0 V	557 mF cm^{-2}, 2 mA cm^{-2}	68.3 % after 5000	3.88 Wh m^{-2}	[18]
e-C-ZnSi-4//AC HSC	PVA/KOH	1.6 V	645 mF cm^{-2}, 2 mA cm^{-2}	75.3 % after 5000	4.80 Wh m^{-2}	[18]
e-C-MnSi-4//AC HSC	PVA/KOH	1.0 V	623 mF cm^{-2}, 2 mA cm^{-2}	76.4 % after 5000	4.41 Wh m^{-2}	[18]
C-NiSi-3//AC HSC	PVA/KOH	1.5 V	409 mF cm^{-2}, 2 mA cm^{-2}	83 % after 5000	2.44 Wh m^{-2}	[19]
C-CoSi-3//AC HSC	PVA/KOH	1.5 V	376 mF cm^{-2}, 2 mA cm^{-2}	79 % after 5000	2.01 Wh m^{-2}	[19]
e-C-NiSi-3//AC HSC	PVA/KOH	1.5 V	444 mF cm^{-2}, 2 mA cm^{-2}	87 % after 5000	3.71 Wh m^{-2}	[19]
e-C-CoSi-3//AC HSC	PVA/KOH	1.5 V	407 mF cm^{-2}, 2 mA cm^{-2}	84 % after 5000	2.59 Wh m^{-2}	[19]
m-C-ZnSi//AC HSC	**PVA/KOH**	**1.6 V**	**681 mF cm^{-2}, 2 mA cm^{-2}**	**83.4 % after 6000**	**5.06 Wh m^{-2}**	**This work**
m-C-MnSi//AC HSC	**PVA/KOH**	**1.0 V**	**648 mF cm^{-2}, 2 mA cm^{-2}**	**85.0 % after 6000**	**4.80 Wh m^{-2}**	**This work**
m-C-NiSi//AC HSC	**PVA/KOH**	**1.5 V**	**512 mF cm^{-2}, 2 mA cm^{-2}**	**85.4 % after 5000**	**4.38 Wh m^{-2}**	**This work**
mC-CoSi//AC HSC	**PVA/KOH**	**1.5 V**	**497 mF cm^{-2}, 2 mA cm^{-2}**	**81.8 % after 5000**	**4.05 Wh m^{-2}**	**This work**

ASC = Asymmetric Supercapacitor; PVA = Polyvinyl Alcohol

References

[1] J. Zheng, Y. Zhang, Q. Wang, H. Jiang, Y. Liu, T. Lv, C. Meng, Hydrothermal encapsulation of VO_2(A) nanorods in amorphous carbon by carbonization of glucose for energy storage devices, Dalton Trans 47 (2018) 452-464.

[2] Y. Zhang, W. Zhou, H. Yu, T. Feng, Y. Pu, H. Liu, W. Xiao, L. Tian, Self-templated synthesis of nickel silicate hydroxide/reduced graphene oxide composite hollow microspheres as highly stable supercapacitor electrode material, Nanoscale Research Letters 12 (2017) 325.

[3] T. Chen, Z. Shifeng, L. Qingshan, Self-templated synthesis of mesoporous manganese silicates as an electrode material for supercapacitor, Ceramics International 44 (2018) 17007-17012.

[4] H. Wang, Y. Wang, X. Bai, H. Yang, J. Han, N. Lun, Y. Qi, Y. Bai, Manganese silicate drapes as a novel electrode material for supercapacitors, RSC Advances 6 (2016) 105771-105779.

[5] Q. Rong, L. Long, X. Zhang, Y. Huang, H. Yu, Layered cobalt nickel silicate hollow spheres as a highly-stable supercapacitor material, Applied Energy 153 (2015) 63-69.

[6] P. Chaturvedi, A. Kumar, A. Sil, Y. Sharma, Cost effective urea combustion derived mesoporous-Li_2MnSiO_4 as a novel material for supercapacitors, RSC Advances 5 (2015) 25156-25163.

[7] Q. Wang, Y. Zhang, H. Jiang, T. Hu, C. Meng, In situ generated $Ni_3Si_2O_5(OH)_4$ on mesoporous heteroatom-enriched carbon derived from natural bamboo leaves for high-performance supercapacitors, ACS Applied Energy Materials 1 (2018) 3396-3409.

[8] G. Zhang, Y. Zhao, F. Tao, H. Li, Electrochemical characteristics and impedance spectroscopy studies of nano-cobalt silicate hydroxide for supercapacitor, Journal of Power Sources 161 (2006) 723-729.

[9] J. Zhao, Y. Zhang, T. Wang, P. Li, C. Wei, H. Pang, Reed leaves as a sustainable silica source for 3D mesoporous nickel (cobalt) silicate architectures assembled into ultrathin nanoflakes for high-performance supercapacitors, Advanced Materials Interfaces 2 (2015) 1400377.

[10] Y. Cheng, Y. Zhang, Q. Wang, C. Meng, Synthesis of amorphous $MnSiO_3$/graphene oxide with excellent electrochemical performance as supercapacitor electrode, Colloids and Surfaces A Physicochemical and Engineering Aspects 562 (2018) 93-100.

[11] Y. Zhang, C. Wang, H. Jiang, Q. Wang, J. Zheng, Cobalt-nickel silicate hydroxide on amorphous carbon derived from bamboo leaves for hybrid supercapacitors, Chemical Engineering Journal 375 (2019) 121938-121938.

[12] Y. Chen, Y. Hsu, Y. Lin, Y. Lin, Y. Horng, L. Chen, K. Chen, Highly flexible supercapacitors with manganese oxide nanosheet/carbon cloth electrode, Electrochimica Acta 56 (2011) 7124-7130.

[13] Q. Wang, Y. Zhang, H. Jiang, X. Li, Y. Cheng, G. Meng, Designed mesoporous hollow sphere architecture metal (Mn, Co, Ni) silicate: A potential electrode material for flexible all solid-state asymmetric supercapacitor, Chemical Engineering Journal 362 (2019) 818-829.

[14] D. Ge, L. Yang, L. Fan, C. Zhang, X. Xiao, Y. Gogotsi, S. Yang, Foldable supercapacitors from triple networks of macroporous cellulose fibers, single-walled carbon nanotubes and polyaniline nanoribbons, Nano Energy 11 (2015) 568-578.

[15] S. Zhang, Y. Liu, J. Zheng, Y. Mu, C. Meng, Rice-like and rose-like zinc silicates anchored on amorphous carbon derived from natural reed leaves for high-performance supercapacitors, Dalton Transactions 50 (2021) 9438-9449.

[16] Y. Zhang, C. Wang, H. Jiang, Q. Wang, J. Zheng, C. Meng, Cobalt-nickel silicate hydroxide on amorphous carbon derived from bamboo leaves for hybrid supercapacitors, Chemical Engineering Journal

375 (2019) 121938-121938.
[17] Y. Zhang, C. Wang, X. Dong, H. Jiang, C. Huang, Alkali etching metal silicates derived from bamboo leaves with enhanced electrochemical properties for solid-state hybrid supercapacitors, Chemical Engineering Journal 417 (2020) 127964-127976.
[18] S. Zhang, J. Zheng, J. Meng, Y. Zhang, F. Niu, Y. Wang, H. Yan, Z. Li, C. Meng, Alkali etching zinc and manganese silicates derived from natural green algaes for supercapacitors with enhanced electrochemical properties, Journal of Colloid and Interface Science 623 (2022) 135-145.
[19] S. Zhang, H. Yan, Y. Wang, F. Niu, T. Guo, Y. Zhang, Z. Li, X. Chun, C. Meng, Butterfly-like metal-silicates derived from natural green algaes for supercapacitors with enhanced electrochemical properties by alkali etching, Journal of Analytical and Applied Pyrolysis, 167 (2022) 105687.